

Fig. S1 Body kinematics of a strike maneuver. (A-E) Rotational and translational dynamics of one trial ($\theta_p \sim 160^\circ$). The shaded interval highlights the maneuvering phase during which period the spider completes one smooth rotation. (A) Rotational velocities, showing a major peak of speed mid-maneuver. (B) Temporal shifts in the orientation of the rotational axis with respect to body-fixed frame. (C) Angular distances traveled by each principle rotation. (D) Translational velocity of body frame. (E) Linear distance travelled by body frame. (F) Relative proportions of each principal rotation during the maneuvering phase (means \pm s.e.m.). The spider body mainly performs positive yaw and negative roll to reorient, which is accompanied by positive (nose-up) pitch. (G) 3D reconstruction of body frame orientation during the strike maneuver of the same trial in (A-E), where the disc represents the X_b - Y_b plane, and red arrows represent positive X_b direction. Left, top view; right, oblique view.

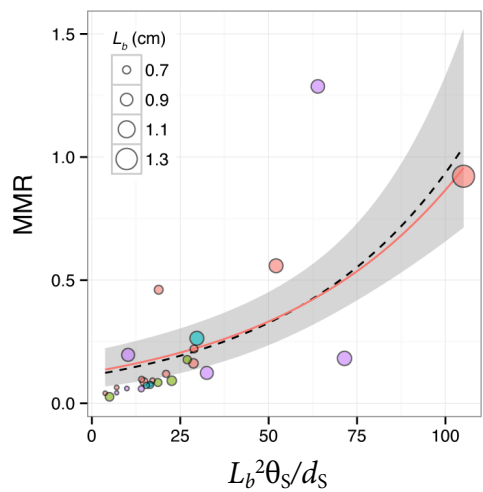


Fig. S2 Maneuver momenta ratio (MMR) plotted against $(L_b^2 \theta_s)/d_s$, showing that the spiders generate greater energy output when striking farther and more posteriorly oriented prey. L_b , body length; θ_s , angle of reorientation; d_s , linear distance of prey to initial spider COM.

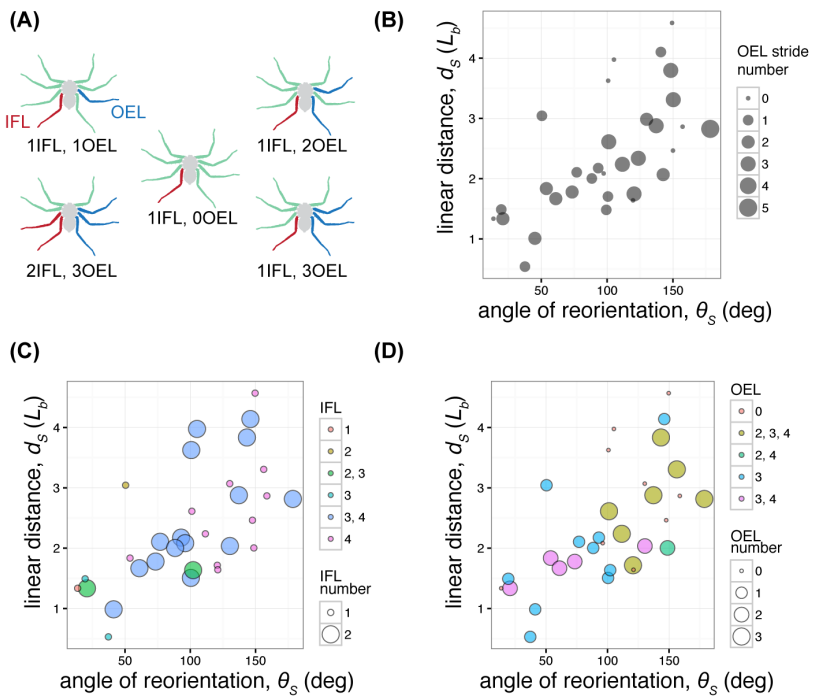


Fig. S3 Gait patterns of strike maneuvers. (A) Demonstrations of various combinations of IFL and OEL. (B) The number of OEL strides plotted against linear distance (d_s) and angular distance (θ_s). Based on generalized linear regression models the number of OEL strides is not correlated with either distances. (C) Different combinations of IFL plotted against d_s and θ_s . Colors represent different IFL combinations; point size represents the number of IFL. (D) Different OEL combinations mapped against d_s and θ_s . Based on generalized linear regression models, the number and combinations of IFL and OEL are not correlated with d_s and θ_s . Kinematics is based on left-turn configuration (see Methods).

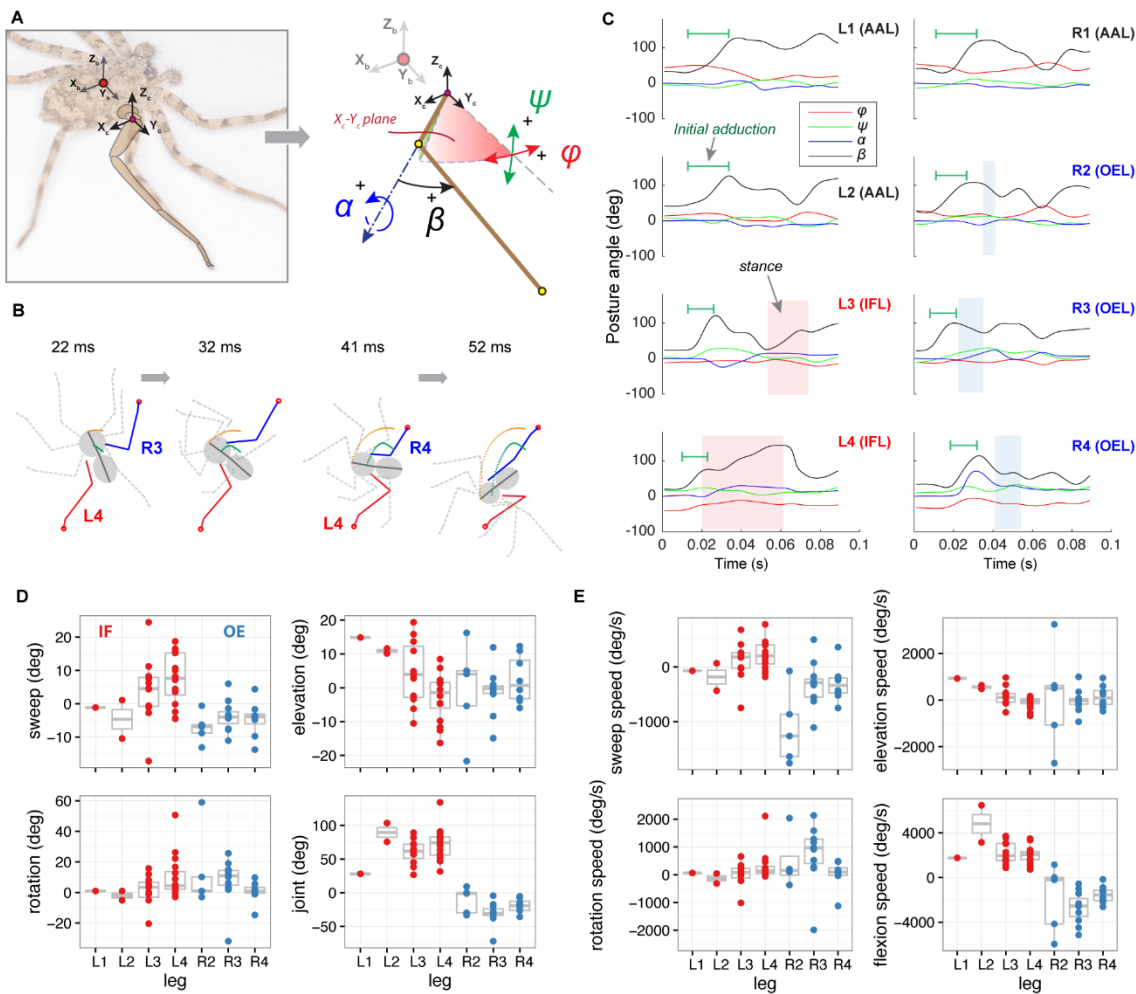


Fig. S4 Three-dimensional leg joint kinematics. (A) Configuration of leg posture angles, demonstrated with leg III. The coxa-fixed coordinate frame has principal axes parallel to those of the body-fixed frame. Four angles describe leg posture: ϕ , sweep angle; ψ , elevation angle; α , rotation angle; β , FP-joint angle. (B) Mid-maneuver sequences of body and leg postures in top view. (C) Dynamics of leg posture angles from the same trial shown in (B). Green segmented lines show initial flexion of FP-joints at the beginning of the maneuver. Shaded areas represent stance. (D) Summary of amplitude of joint rotations for each posture angle for IF and OE actions. (E) Summary of joint rotation speeds for IFL and OEL actions. Kinematics is based on left-turn configuration (see Methods).

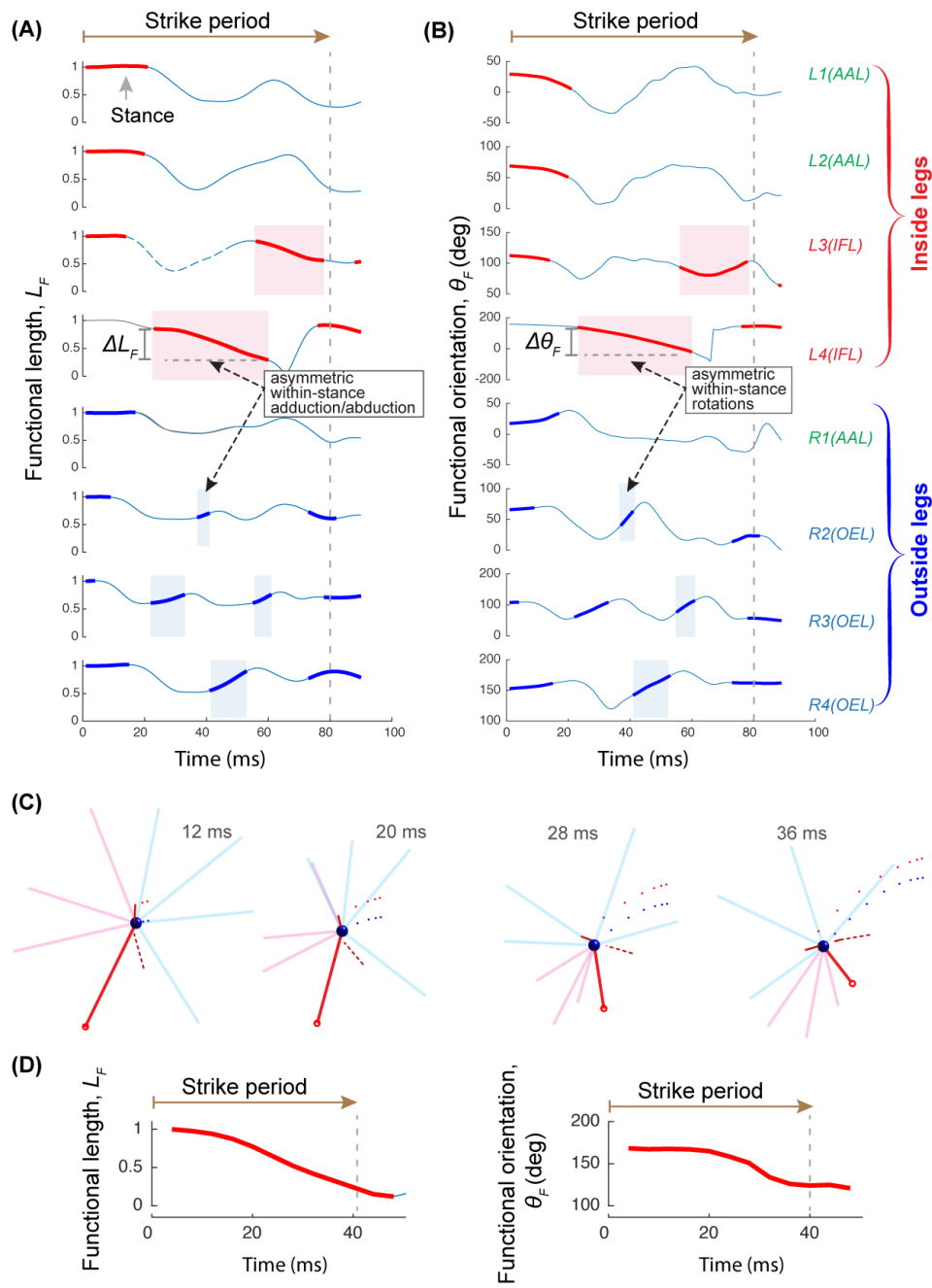


Fig. S5 Kinematics of leg deformations. (A)-(B) Dynamics of functional leg length (initial size normalized) and functional orientation (θ_F) of the same trial in Fig. 5E. Shaded intervals represent stance. Red, inside legs; blue, outside legs; thickened segments of lines represent stance. (C)-(D), Kinematics of leg deformations for a strike driven by a single IFL (left leg IV). (C) Strike sequence in functional leg representation. (D) Temporal dynamics of functional leg length (initial size normalized) and functional orientation of left leg IV. Kinematics is based on a left-turn configuration.

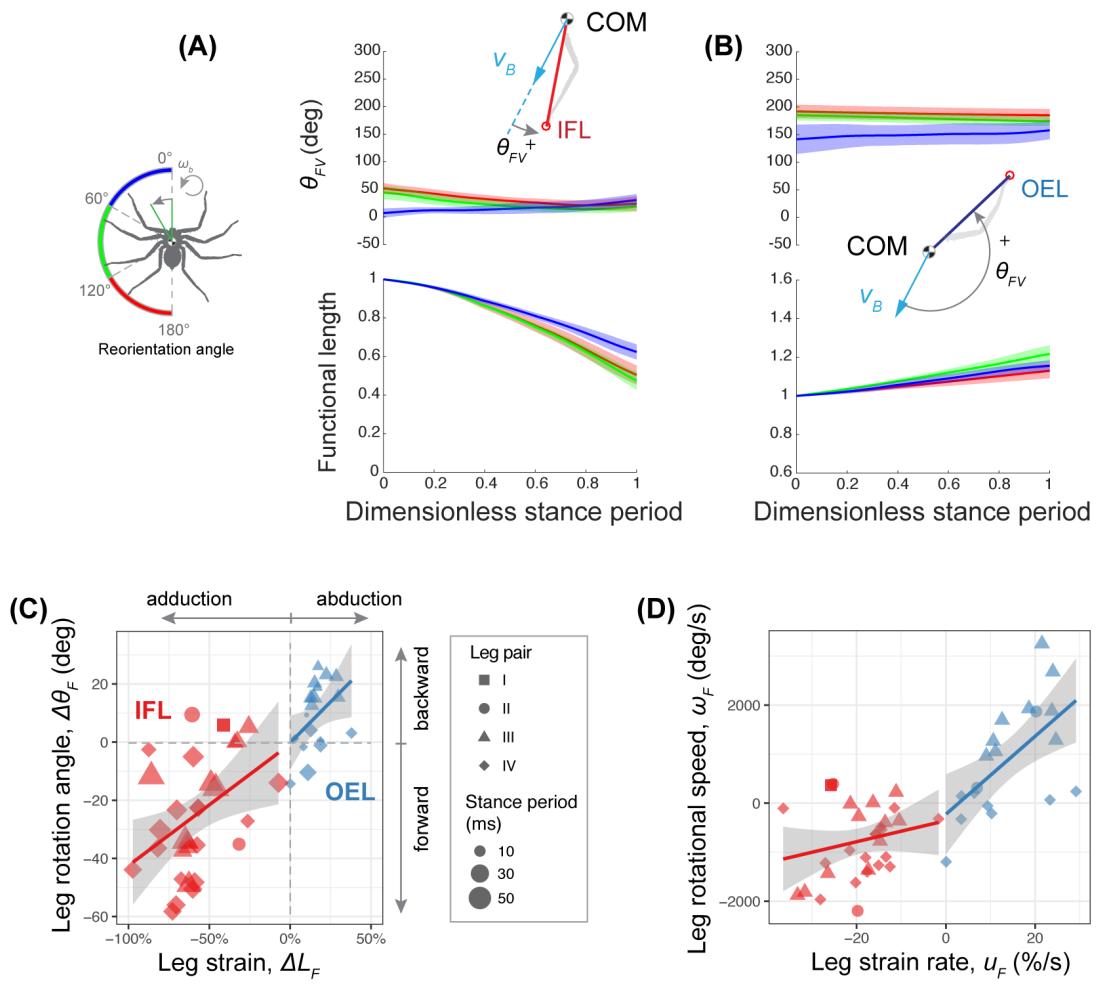


Fig. S6 Comparison of deformation kinematics between four leg pairs. (A) Dynamics of functional orientation and length variation during stance of IFL, showing shortening (i.e., adduction) and forward rotation in the leading side of COM heading. Color represents the three ranges of the total reorientation angle. θ_{FV} , leg functional orientation vs. COM velocity v_B , with counter-clockwise as the positive direction. (B) Dynamics of functional length and orientation variation during stance of OEL, which performs lengthening (i.e., abduction) in the trailing side of COM velocity. (C) Correlation between the degree of abduction/adduction (ΔL_F) and rotation amplitude ($\Delta\theta_F$), showing the coupling between abduction/adduction and rotations. Trend lines represent generalized linear models; shaded areas represent s.e.m. (D) Correlations between the rate of abduction/adduction (u_F) and rotation speed (ω_F). (C) and (D) suggest kinematics templates of within-stance deformation were shared by legs playing the same roles for strike maneuver. (C) and (D), $P<0.01$ for all correlations based on a generalized linear regression model.

Tables

	L_L/L_b	L_1/L_2
Leg I	1.3 ± 0.3	1.95 ± 0.19
Leg II	1.9 ± 0.6	1.9 ± 0.22
Leg III	1.4 ± 0.3	1.99 ± 0.12
Leg IV	2 ± 0.5	1.86 ± 0.27

Table S1. Length ratio between body and leg sections. L_L/L_b , leg length to body (cephalothorax and abdomen) length ratio. L_1/L_2 , length ratio of section 1 to section 2 (Fig. 2A). Values are means±s.d.

Body parts	Mass percentage
Cephalothorax	32.7 ± 4.98
Abdomen	23.3 ± 6.21
Leg I	a 0.54 ± 0.38
	b 2.84 ± 0.97
	c 6.32 ± 1.45
Leg II	a 0.51 ± 0.47
	b 3.92 ± 0.99
	c 7.91 ± 1.54
Leg III	a 0.85 ± 0.59
	b 3.48 ± 0.98
	c 7.7 ± 1.79
Leg IV	a 0.8 ± 0.54
	b 2.69 ± 1.26
	c 6.45 ± 1.54

Table S2. Mass distribution of body sections (*S. wilsoni*, $N=5$; *S. debilis*, $N=5$). Values are mass percentages with respect to total (means±S.D.). See Fig. S2 for partitioning of leg sections for mass distribution measurement. Leg sections: a, tarsus and metatarsus; b, tibia; c, femur. Mass percentages of each leg section represent single sections.

Taxa		Strike direction	Medium	Prey cues	Period	Linear speed	Linear distance	Reference
mantis shrimp	<i>Lysiosquillina maculata</i>	forward	Water	visual, chemosensory	24.98±9.68 ms		~2.2% to 6.7% L_b	deVries et al., 2012
	<i>Alachosquilla vicina</i>	forward	Water		3.26±0.41 ms		~25.3% to 50.1% L_b	deVries et al., 2012
	<i>Odontodactylus scyllarus</i>	forward	Water			14 to 23 m/s		Patek et al., 2004
snake	Shedao pit-viper (<i>Gloydius shedaoensis</i>)	forward, straight upward	Air	visual, thermal		0.5 to 2.5 m/s	>20 cm, or 25% L_b	Shine et al., 2002; Shine and Sun, 2002
	Pacific rattlesnake (<i>Crotalus viridis</i>)	forward	Air					Kardong, 1986
	Couch's garter snake (<i>Thamnophis couchii</i>)	forward	Water	visual		1.12 m/s (mean peak speed)	2 to 12 cm, or 4% to 20% L_b	Alfaro, 2002
	Tentacled snake (<i>Erpeton tentaculatus</i>)	lateral to head	Water	mechanical	30 to 40 ms	~1.1 m/s (mean)	0.8 to 3.0 cm, or 3% to 12% L_b	Smith et al., 2002; Catania, 2009
spider	crab spider (<i>Misumena vatia</i>)	forward	Air	visual, mechanical				Morse, 1981
	trapdoor spider (<i>Aliatypus</i> sp.)	forward	Air	mechanical	30 to 130 ms		5 mm maximum	Coyle and Icenogle, 1994
	flattie spider (<i>Selenops</i> spp.)	omnidirectional (Fig. 3)	Air	visual, mechanical	52 to 116 ms	0.2 to 0.6 m/s (or 10 to 80 L_b /s)	100% to 500% L_b	present study

Table S3. Comparison of strike performance between different ambush predators. *, calculated based on data from cited literature. L_b , body length. This comparison shows flattie spiders perform fast strikes that cover angular and linear ranges greater than other ambush predators.

Taxa	Turning performance	Heading angle change; longitudinal axis rotation (deg)	Linear speed (cm/s, L_b/s)	Angular speed (deg/s) (mean; maximum)	Curvature (cm $^{-1}$)	Number of strides	Body length (cm)	Body mass (g)	Reference
Death-head cockroach (<i>Blaberus discoidalis</i>)	during running	48; 40	20; 4.5	157	0.8	3.6	4.4	4.6	Jindrich and Full, 1999; Kram et al., 1997
Mite (<i>Paratarsotomus macropalpis</i>)	during running; with pivot leg	~; 103	2.4; 21	795; 1253	5.8	3.4	0.114	2.5×10^{-5} to 2.5×10^{-4}	Rubin et al., 2016
	during running; without pivot leg	~; 102	2.9; 27.4	567; 1040	3.4	4	0.106		
Fruitfly (<i>Drosophila melanogaster</i>)	tight turn	~; 100		400 (single trial)			0.25		Strauss and Heisenberg, 1990
Honeybee (<i>Apis mellifera</i>)	tight turn	~; 180		157	0.89		1.6		Zolotov et al., 1975
Flattie spider (<i>Selenops</i> spp.)	ambush turn	<10–50; 10–160	10–60; 10–80 (Fig.4)	~; ~3000 (Fig.4)	2.54 ± 6.54 (mean \pm SD)	0–1 (inside leg); 0–3 (outside leg)	0.5–1.4	0.019–0.279	present study

Table S4. Comparison of turning maneuvers in arthropods. Here turning maneuver specifically refers to the reorientation of body longitudinal axis along the substrate, mostly consisting of yaw. Values were calculated based on data from the original reference if necessary. ‘~’ represents missing data or non-applicable. This comparison also shows flattie spiders perform fast turning maneuvers with fewer strides than other animals.

Effects	Coefficients (s.e.)	T value	P value
Strike reorientational speed (deg/s)			
Prey angular distance (deg)	13.6 (1.2)	11.3	<0.001
Body size (cm)	-536.1 (213.0)	-2.5	<0.05
Body size – normalized strike linear speed (L_b/s)			
Prey linear distance (cm)	12.3 (1.6)	7.6	<0.001
Body size (cm)	-17.5 (6.2)	-2.8	<0.01

Table S5. Summary of multiple regression analyses addressing the effects of prey distance and body size to strike speed, including both angular and linear components.

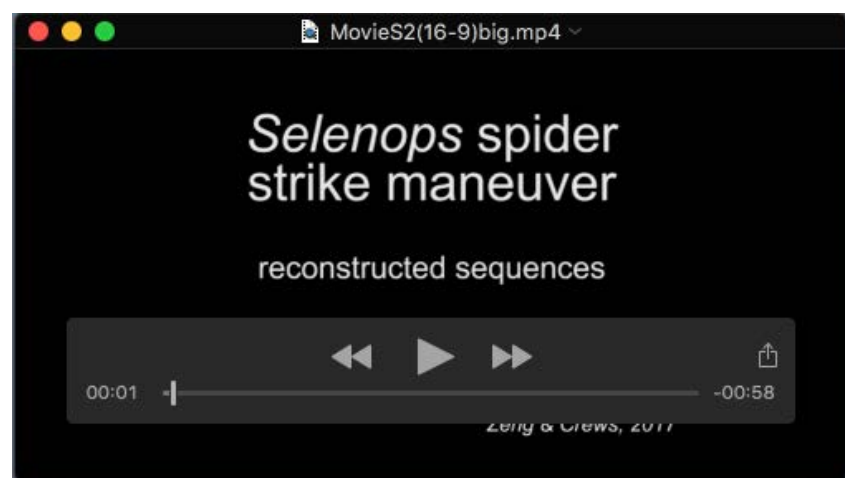
Supplementary References

- Alfaro, M. E.** (2002). Forward attack modes of aquatic feeding garter snakes. *Functional Ecology* **16**, 204-215.
- Catania, K. C.** (2009). Tentacled snakes turn C-starts to their advantage and predict future prey behavior. *Proc Natl Acad Sci U S A* **106**, 11183-11187.
- Coyle, F. A. and Icenogle, W. R.** (1994). Natural history of the Californian trapdoor spider genus *Aliatypus* (Araneae, Antrodiaetidae). *Journal of Arachnology*, 225-255.
- deVries, M. S., Murphy, E. A. and Patek, S. N.** (2012). Strike mechanics of an ambush predator: the spearing mantis shrimp. *J Exp Biol* **215**, 4374-4384.
- Jindrich, D. L. and Full, R. J.** (1999). Many-legged maneuverability: dynamics of turning in hexapods. *J Exp Biol* **202**, 1603-1623.
- Kardong, K. V.** (1986). The predatory strike of the rattlesnake: when things go amiss. *Copeia* **1986**, 816-820.
- Kram, R., Wong, B. and Full, R. J.** (1997). Three-dimensional kinematics and limb kinetic energy of running cockroaches. *J Exp Biol* **200**, 1919-1929.
- Morse, D. H.** (1981). Prey capture by the crab spider *Misumena vatia* (Clerck) (Thomisidae) on three common native flowers. *American Midland Naturalist*, 358-367.
- Patek, S. N., Korff, W. L. and Caldwell, R. L.** (2004). Deadly strike mechanism of a mantis shrimp. *Nature* **428**, 819-820.
- Rubin, S., Young, M. H., Wright, J. C., Whitaker, D. L. and Ahn, A. N.** (2016). Exceptional running and turning performance in a mite. *J Exp Biol* **219**, 676-685.
- Shine, R., Sun, L. -X., Fitzgerald, M., Kearney, M. and Guyer, C.** (2002). Antipredator responses of free-ranging pit vipers (*Gloydius shedaoensis*, Viperidae). *Copeia* **2002**, 843-850.
- Shine, R. and Li-Xin, S.** (2002). Arboreal ambush site selection by pit-vipers *Gloydius shedaoensis*. *Animal Behaviour* **63**, 565-576.
- Smith, T. L., Povel, G. D. E. and Kardong, K. V.** (2002). Predatory strike of the tentacled snake (*Erpeton tentaculatum*). *Journal of Zoology* **256**, 233-242.
- Strauss, R. and Heisenberg, M.** (1990). Coordination of legs during straight walking and turning in *Drosophila melanogaster*. *J Comp Physiol A* **167**, 403-412.
- Zolotov, V., Frantsevich, L. and Falk, D. -I. E. -M.** (1975). Kinematik der phototaktischen Drehung bei der Honigbiene *Apis mellifera* L. *Journal of comparative physiology* **97**, 339-353.



Supplementary movie 1

Four sample clips of strike maneuvers.



Supplementary movie 2

Reconstructed strike maneuver sequences. For skeletal view, body and leg sections are shown as line segments; red dotted lines represent trajectories of the anterior end; black dotted lines represent trajectories of the spider's center of mass; red circles indicate substrate contact. For 'functional leg' representation, the blue sphere represents spider center of mass; red dotted lines are trajectories of the anterior end; blue dotted lines are trajectories of spider center of mass; red circles indicate substrate contact.